Inhibition of Hsp90 in the spinal cord enhances the antinociceptive effects of morphine by activating an ERK–RSK pathway

David I. Duron[1], Wei Lei[1], Natalie K. Barker[2], Carrie Stine[1], Sanket Mishra[3], Brian S. J. Blagg[3], Paul R. Langlais[2], and John M. Streicher[1*]

[1]Department of Pharmacology, College of Medicine, University of Arizona, Tucson AZ USA 85724.

[2]Department of Medicine, Division of Endocrinology, College of Medicine, University of Arizona, Tucson AZ USA 85724.

[3]Department of Chemistry and Biochemistry, College of Science, University of Notre Dame, Notre Dame IN USA 46556.

*Corresponding author. Email: JStreicher@email.arizona.edu.

Abstract:

Morphine and other opioids are commonly used to treat pain, despite their numerous adverse side effects that include respiratory depression, addiction, and tolerance. The modulation of μ-opioid receptor (MOR) signaling is one way to potentially improve opioid therapy. Heat shock protein 90 (Hsp90) is a molecular chaperone protein that has been shown to mediate MOR signaling within the brain in mice. Here, we found that the inhibition of Hsp90 specifically within the spinal cord enhanced morphine-induced anti-nociception. Intrathecal, but not systemic, administration of the Hsp90 inhibitors 17-AAG or KU-32 amplified the effects of morphine in suppressing both thermal and mechanical sensitivity in mice. Furthermore, Hsp90 inhibition enabled phosphorylation of the kinase ERK in response to opioid treatment. ERK activation was localized within the dorsal horns of the spinal cord, which are heavily populated with primary afferent sensory neurons. The additive effects of Hsp90 inhibition were abolished upon intrathecal inhibition of ERK or protein synthesis. Quantitative proteomic analysis identified upregulated abundance of the kinase RSK after Hsp90 inhibition in the spinal cord; intrathecal inhibition of RSK with a small molecule inhibitor blocked the additive effects of Hsp90 inhibitors on morphine-induced anti-nociception. This identified ERK/RSK cascade downstream of MOR, localized to the spinal cord and repressed by Hsp90, may be used to enhance the efficacy and presumably decrease the side effects of opioid therapy.

Introduction

Currently available therapeutics for the treatment of chronic pain are largely limited by their efficacy and undesired side effects. With over 100 million individuals affected and an economic burden exceeding $600 billion in the United States alone, chronic pain remains an area of critical and growing medical need (1, 2). One of the more efficacious treatment options are opioid analgesics, such as morphine. Although these drugs can be very effective acutely, their side effects such as tolerance, addiction, and respiratory depression make them a high-risk choice when dealing with long-term medication regimens (3, 4). Accompanying these negative side effects is a growing social awareness of the potential dangers of opioids that have begun to negatively stigmatize their use, abetted by a growing opioid abuse and addiction crisis (5).

Intensive decades-long research has revealed a complex signaling network evoked by opioid treatment downstream of the μ-opioid receptor (MOR) (6). Increased understanding of the complexity of MOR signal transduction has resulted in new efforts for drug discovery and development, such as biased agonism to reduce opioid side effects (7-9). These efforts have produced new biased ligands, as well as additional drugs targeting key proteins such as the kinase mTOR or MOR signaling-relevant receptors, such as PAR2, to either augment or reduce key behavioral outputs, such as anti-nociception (10-14). These efforts illuminate the relevant MOR signaling cascades beyond the "classical" $G\alpha_I$ cascade and show the value in elucidating key downstream signaling regulators.

Heat shock protein 90 (Hsp90) is a molecular chaperone protein that is upregulated in response to stress. It regulates its client proteins via several molecular mechanisms, including protein folding, kinase modulation, protein complex formation, and subcellular localization (15,

16). Hsp90 makes up roughly 2% of the total protein pool in a given cell, highlighting its centrality to cell biology. Its functions have primarily been investigated in the context of cancer (17-19), but Hsp90 has been shown to have a key role in regulating signal transduction at the receptor and downstream cascade levels in a number of different tissues and physiological contexts (20).

In earlier work, we tested the hypothesis that Hsp90 could play a key role in MOR signal transduction by selectively inhibiting Hsp90 in the brain using intracerebroventricular (i.c.v.) administration of 17-N-allylamino-17-demethoxygeldanamycin (17-AAG). In that study, we found that brain Hsp90 inhibition completely suppressed the anti-nociceptive effects of systemically administered morphine in a variety of murine pain models (21). In addition, we showed that i.c.v. administration of 17-AAG blocked the phosphorylation of extracellular signal-regulated kinase (ERK) in response to the selective MOR agonist and synthetic opioid peptide DAMGO ([D-Ala^2, *N*-MePhe^4, Gly-ol]-enkephalin), and that this loss of ERK phosphorylation was responsible for the loss of morphine anti-nociception. Those findings demonstrated that Hsp90 promotes MOR signaling in the brain and identified new signaling pathways to explore further. However, that work left many mechanistic details unknown, as well as the contribution of other regions of the central nervous system like the spinal cord, which may be more applicable clinically due to the potential for intrathecal drug delivery.

Here, we investigated Hsp90 modulation of MOR signal transduction in the spinal cord in mice. Contrary to what was observed in our previous study in the brain, Hsp90 inhibition in the spinal cord amplified the anti-nociceptive effects of morphine. We further identified a molecular mechanism for this effect within the spinal cord dorsal horn. Our findings suggest a potential opioid dose reduction strategy via spinal Hsp90 inhibition to minimize the negative side effects of opioids while maintaining their analgesic benefits.

Results

Inhibition of Hsp90 in the spinal cord enhances morphine-induced anti-nociception

We previously showed that i.c.v.-administered Hsp90 inhibitors completely ablated morphine-induced anti-nociception in multiple pain models (21). In addition, Hsp90 has a considerable number of client proteins, which differ in various tissue, cellular, and environmental contexts (22-24). This suggests the potential for context specific roles for Hsp90 within downstream MOR signaling. We sought to test this role for Hsp90 in MOR signaling by considering the contribution of Hsp90 to morphine-induced anti-nociception within the spinal cord. CD-1 mice were treated with intrathecally (i.t.)-administered 17-AAG, a geldanamycin derivative which competitively binds the N-terminal ATP binding domain of Hsp90. 24 hours after injection, mice were then treated with 3.2 mg/kg morphine subcutaneously (s.c.), and behavioral pain assays were performed.

Contrary to our previous report with i.c.v. administered 17-AAG, we found that spinally inhibited Hsp90 resulted in an increased anti-nociceptive response (meaning, less pain-evoked sensitivity) due to morphine in both thermal tail flick and mechanical post-operative paw incision pain models (**Fig. 1A-B**). To verify the Hsp90 selectivity of these results, we utilized a C-terminal inhibitor of Hsp90, KU-32, that binds to an alternate site than 17-AAG, and thus is unlikely to share off-target interactions (25, 26). KU-32 was administered to the spinal cord followed by subcutaneous morphine 24 hours later. Enhanced morphine-induced anti-nociception was also observed with KU-32 treatment, confirming the Hsp90 selectivity of our results (**Fig. 1C**).

We next confirmed that these findings were not due to off-target motor or sedative effects using the Rotarod test. Spinal 17-AAG treatment had no impact on Rotarod performance in the mice, suggesting that our findings reflect *bona fide* changes to the opioid pain modulatory system (**Fig. 1D**). Lastly, in our previous report, we tested the brain role of Hsp90 in tail flick pain using i.c.v. DAMGO instead of morphine, showing that inhibition of brain Hsp90 had no impact on tail flick pain (21). To confirm that our tail flick results here were due to changes in Hsp90 location (brain vs. spinal cord) rather than drug and route (i.c.v. DAMGO vs. s.c. morphine), we tested i.c.v. 17-AAG combined with s.c. morphine. We found that at both 3.2 and 10 mg/kg s.c., morphine had no impact on tail flick response (**Fig. 1E**), the same as for i.c.v. DAMGO in our earlier study (21).

Inhibition of Hsp90 in the brain overrides inhibition in the spinal cord

With behavioral differences identified in brain vs. spinal cord Hsp90 inhibition, we next tested the interaction of these two regions using systemic Hsp90 inhibition, which would impact both brain and spinal cord. To do this we injected mice with intraperitoneal (i.p.) 17-AAG and assessed its effects on morphine induced anti-nociception after a 24-hour period. We tested for increased Hsp70 expression levels as a marker of Hsp90 inhibition within the periaqueductal grey (PAG) brain region and spinal cord tissue post 24 hours i.p. 17-AAG using Western blot (21). We found that Hsp70 levels were increased in the PAG as expected, validating our treatment regimen as effective in inhibiting CNS Hsp90 (**Fig. 2A-B**). Unexpectedly, we were unable to detect an increase in spinal cord Hsp70 (**Fig. 2A-B**). 17-AAG was likely reaching the spinal cord since we've shown it can reach the PAG, thus this result may represent different molecular mechanisms for Hsp90 in the brain vs. the spinal cord. Now validated, we tested the impact of systemic 17-

AAG on morphine anti-nociception. We observed that systemic delivery of 17-AAG had no impact on anti-nociception in the tail flick pain model and markedly reduced anti-nociception in the paw incision pain model (**Fig. 2C-D**); these results are very similar to what was observed with i.c.v. 17-AAG treatment previously (21) as well as here (**Fig. 1E**).

The effects on morphine anti-nociception seen with systemic Hsp90 inhibition suggest that the signaling events within the brain may override that of the spinal cord. To directly test this hypothesis and rule out peripheral mechanisms, we performed dual i.c.v. and i.t. injections of 17-AAG. We found that dual brain and spinal cord injections recapitulated systemic injection in both the tail flick and paw incision pain models (**Fig. 2E-F**). These results suggest that the signaling events regulated by Hsp90 within the brain override MOR signaling within the spinal cord, which would otherwise allow for amplified pain relief in these models.

ERK MAPK signaling is activated by spinal Hsp90 inhibition and mediates enhanced anti-nociception

Our previous study within the brain demonstrated that blocked activation of ERK MAPK in the PAG by 17-AAG treatment is a mechanism for the reduction in morphine induced anti-nociception (21). We thus tested ERK signaling activation within the spinal cord after i.t. 17-AAG and DAMGO (selective MOR agonist) treatment using Western blot. DAMGO was used as a high efficacy selective agonist, increasing our ability to observe kinase changes in tissue vs. the partial agonist morphine; our results above (**Fig. 1E**) and experiments below validate this choice. Notably, DAMGO alone showed no ERK activation relative to vehicle treatment; in contrast, 17-AAG induced an elevated ERK baseline with a further increase in ERK phosphorylation when combined with DAMGO (**Fig. 3A-B**). As in our systemic inhibition studies above, we also sought to confirm

Hsp90 inhibition by 17-AAG by testing for Hsp70 upregulation (21, 27, 28). We again found no Hsp70 upregulation, even with direct i.t. injection of inhibitor, confirming our systemic results above and further suggesting that Hsp90 molecular mechanisms may differ in the spinal cord vs. the brain (**Fig. 3A, C**).

To localize the observed increases in ERK phosphorylation within the spinal cord, we performed immunohistochemical (IHC) analysis of spinal cord tissue from mice treated with i.t. 17-AAG and DAMGO as for our Western studies. Our findings confirmed the Western results, with very low phospho-ERK signal observed in vehicle-only treated mice (Vehicle/Vehicle; order of treatment denoted by /) and vehicle followed by DAMGO-treated mice (Vehicle/DAMGO); we observed some increase in signal in the 17-AAG/Vehicle group, and a large increase in specific phospho-ERK signal in the 17-AAG/DAMGO group (**Fig. 3D**). We particularly noted an apparent increase in ERK phosphorylation in the lamina I/II region of the dorsal horn, a region rich in nociceptive input and opioid receptors (**Fig. 3D,** white arrows). We also performed co-localization studies with NeuN, a marker for neuronal cell bodies, and MAP2, a neuronal cytoskeletal protein enriched in dendrites; we found that the pERK signal co-localized with MAP2 but not NeuN, suggesting ERK activation in post-synaptic dendrites (**Fig. 3E**). This was confirmed using high magnification imaging (**Fig. 3F)**, in which substantial but not complete pERK/MAP2 overlap was detected. We also quantitated the pERK signal in the dorsal horn region, which confirmed a significant increase with 17-AAG and DAMGO co-treatment (**Fig. 3G**).

To investigate whether these differences in ERK signaling contribute to the enhanced morphine-induced anti-nociception observed, we performed behavioral analysis with co-treatment of i.t. 17-AAG and i.t. U0126, a MEK/ERK inhibitor. In both tail flick and paw incision models, U0126 treatment brought the enhanced morphine-induced anti-nociceptive profile back to the

baseline morphine response (**Fig. 3H-I**). In addition, mice treated with U0126 alone without 17-AAG showed no difference in morphine induced anti-nociception (**Fig. 3H-I**). These results demonstrate that ERK phosphorylation within the spinal cord is necessary for increased morphine induced anti-nociception via spinal cord Hsp90 inhibition. They also support our Western and IHC results suggesting that ERK is not activated by opioids without Hsp90 inhibition.

Rapid protein translation after ERK activation mediates enhanced morphine anti-nociception after spinal inhibition of Hsp90

Hsp90 and ERK MAPK signaling pathways have been previously connected to translational initiation (29-32). To evaluate the possibility of these pathways altering translation and subsequently contributing to the behavioral differences observed here, we administered the translational inhibitor cycloheximide (CX) i.t. in the context of our behavioral experiments. In a very similar pattern to the ERK inhibitor experiments above, we found that CX, 24 hours post-17AAG and 30 minutes prior to morphine, reduced the enhancement of morphine induced anti-nociception back to baseline in the tail flick model (**Fig. 4A**). CX alone without 17-AAG treatment did not change morphine-induced anti-nociception (**Fig. 4A**). These findings suggest that rapid translation within 30 minutes of opioid treatment is necessary for the enhanced morphine anti-nociception seen through spinally inhibited Hsp90.

To identify the position of translation within the Hsp90/ERK molecular cascade, we performed Western blot analysis on spinal cord tissues harvested from mice treated with 17-AAG and combinations of CX and DAMGO. 17-AAG paired with DAMGO treatment stimulated ERK phosphorylation as above; CX treatment 30 minutes prior to DAMGO had no effect on this

stimulation (**Fig. 4B-C**). These results suggest that translational initiation is a downstream event from ERK phosphorylation after Hsp90 inhibition.

Proteomic analysis reveals a protein network altered by spinal Hsp90 inhibition

Our results above suggest that protein translation is altered by spinal Hsp90 inhibition; these changes should thus in principle be measurable by quantitative proteomics. We treated mice with i.t. 17-AAG or Vehicle control as above for 24 hours and removed their spinal cords for analysis. We followed a protocol of protein extraction, SDS-PAGE gel separation with 6 equal bands excised, tryptic digest, and an MS-MS analysis workflow (**Fig. 5A**). We detected 116 proteins significantly downregulated by 17-AAG treatment and 69 proteins significantly upregulated; unbiased hierarchical clustering analysis showed that the individual mice in each sample group (Vehicle vs. 17-AAG) clustered together, validating a consistent effect of 17-AAG treatment (**Fig. 5B**). The full data sets for the significantly altered proteins in the whole analysis and in the sub-analyses shown in this figure are available in data files S1 and S2. Of the proteins in this data set, we noted that the abundance of the kinase RSK2 was significantly upregulated by 17-AAG treatment (**Fig. 5C**). RSK2 has been shown to promote acute opioid anti-nociception, highlighting this protein as a potential mechanism for spinal Hsp90 inhibition impacting opioid anti-nociception (33).

We next performed additional analyses to validate the proteomic data set and explore the network of protein changes evoked by Hsp90 inhibition. Principal component analysis (PCA) showed that the individual mice in each treatment group (vehicle vs. 17-AAG) clustered together; the groups were strongly separated from each other on Component 1, accounting for 75.1% of the variance; whereas within the same treatment, the samples were much closer together along

Component 2, accounting for only 8.5% of the variance (**Fig. 5D**). We also represented our data in a volcano plot, permitting an overall visualization of significance and fold-change (**Fig. 5E**). Together these analyses further confirm the quality of our data and analysis.

Lastly, we performed Gene Ontology and KEGG Pathways analysis of the significantly changed proteins using Database for Annotation, Visualization, and Integrated Discovery (DAVID) to identify broad themes in functions and processes altered by Hsp90 inhibition. We identified proteins heavily represented in molecular functions such as kinase activity, protein kinase binding, and protein phosphatase binding; pathways including metabolic pathways and oxytocin signaling; processes such as phosphorylation, cell proliferation, lipid metabolism, and synaptic plasticity; and cell components including synapse, exosome, focal adhesion, and postsynaptic density (**Fig. 5F and data file S2**). This network analysis begins to identify an overall role for Hsp90 in regulating protein networks in the spinal cord, which has not been previously reported.

RSK signaling mediates the enhanced anti-nociceptive effects of spinally inhibited Hsp90

Cytosolic RSK1 and RSK2 have both been implicated in translational initiation through several substrates, suggesting a potential link to our translation findings above (34-40). RSK2 has also been implicated in acute morphine induced analgesia within the medial habenula (33). Our proteomic analysis demonstrated altered expression levels of RSK2 within the spinal cord due to Hsp90 inhibition. Therefore, we aimed to probe both RSK1 and RSK2 as a potential mechanism within this molecular pathway.

To evaluate the necessity of RSK activation within our behavioral model, we utilized the irreversible RSK1/2 inhibitor 1-[4-Amino-7-(3-hydroxypropyl)-5-(4-methylphenyl)-7H-pyrrolo[2,3-d] pyrimidin-6-yl]-2-fluoroethanone (Fmk). In a similar design to the U0126 and CX experiments above, 24 hour i.t. 17-AAG was combined with i.t. Fmk 30 minutes before morphine treatment in the tail flick model. Fmk treatment returned the enhanced morphine anti-nociception caused by 17-AAG treatment back to baseline, while Fmk alone without 17-AAG treatment had no effect on morphine anti-nociception (**Fig. 6A**). These results show the same pattern as the U0126 and CX experiments above, and strongly suggest that RSK promotes morphine anti-nociception after spinal Hsp90 inhibition. Notably, Fmk is non-selective between RSK1 and RSK2, so either or both isoforms could promote anti-nociception.

To confirm and extend these findings, we evaluated phosphorylation levels of both isoforms by Western blot in treated spinal cords as above. We found that both RSK1 and RSK2 demonstrate a similar phosphorylation pattern to that of ERK. 17-AAG treatment alone elicits increases in both RSK1 and RSK2 phosphorylation that rises to the level of significance for RSK2; 17-AAG and DAMGO co-treatment significantly increases phosphorylation of both proteins vs. the Vehicle/Vehicle control group, and over the 17-AAG/Vehicle group for RSK2 (**Fig. 6B-D**). These results show that both RSK1 and RSK2 are activated by 17-AAG and DAMGO co-treatment and may both promote morphine anti-nociception after spinal cord Hsp90 inhibition.

Discussion

In this study, we've identified a previously unknown molecular ERK-RSK signaling circuit in the spinal cord which can promote acute opioid-induced anti-nociception; this circuit is normally suppressed by Hsp90 and is only uncovered by spinal Hsp90 inhibition. Our results place rapid

protein translation as a downstream event of ERK activation. Given the extensive literature that has shown an ERK-RSK-translation cascade (34-40), we propose a model by which Hsp90 inhibition relieves the repression of ERK activation by MOR, resulting in an ERK-RSK-translation–mediated cascade facilitating opioid-induced anti-nociception (**Fig. 7**).

Our results provide strong support that spinal ERK, RSK, and translation are not active at baseline for acute opioid anti-nociception. The inhibitors U0126, Fmk, and CX all had no effect on their own without 17-AAG treatment; we also showed that neither ERK nor RSK phosphorylation was stimulated by opioid treatment in vehicle-treated control mice using both Western blot and IHC methods. Notably, we could find no literature reports showing acute activation of these kinases by opioids in the spinal cord. This is in sharp contrast to the brain, where our results and others show that ERK and RSK are phosphorylated by baseline opioid treatment, and contribute to opioid anti-nociception (21, 33, 41-44). This is not to say that ERK can have no impact on the opioid system in the spinal cord. Spinal ERK has been shown to have a role in mediating chronic opioid treatment side effects, particularly tolerance (45). ERK also has a well-established role in promoting chronic pain states after activation in the dorsal horn by strong and chronic pain stimuli (46). These contrasting findings show the importance of context in the function of signaling kinases. ERK is downstream of numerous receptor systems in the same cell and must be able to carry out diverse functions in the same cell when stimulated by these different systems. We propose that ERK is organized uniquely within the spinal cord so that it does not respond to acute MOR activation but is free to act in response to chronic MOR activation and in response to other receptor systems; our results suggest that Hsp90 could be this organizing factor preventing acute activation by the MOR. Removing this blockade enables ERK activation, leading to RSK activation, translation of new proteins, and enhanced anti-nociception. Uncovering these

additional mechanisms will lend great insight into how MOR signaling is organized in the spinal cord.

One potential clue to the unique organization of Hsp90 in the spinal cord is that we found that spinal Hsp90 inhibition does not result in Hsp70 upregulation, confirmed in multiple experiments. Hsp70 upregulation in response to Hsp90 inhibition has long been considered a canonical response, caused by the release of heat shock factor-1 when Hsp90 is inhibited; we and many others have shown in this paper and elsewhere that Hsp70 is upregulated in response to Hsp90 inhibition in numerous cell lines as well as brain tissue (21, 47). Notably, however, we cannot find any reports of Hsp70 upregulation in the wild-type spinal cord in vivo after Hsp90 inhibitor treatment. Others have pointed out that Hsp90 inhibition does not always result in a heat shock response leading to Hsp70 upregulation (48). It may be that Hsp90 in the spinal cord is organized differently at the molecular level than in the brain; perhaps it does not interact with heat shock factor-1 or similar proteins in the spinal cord. These differences may point to the mechanism by which Hsp90 has different signaling roles in brain vs. spinal cord.

Our observations are consistent with the ERK/RSK cascade enhancing opioid activation via rapid protein translation. Hsp90 and ERK have both been linked to the initiation of protein translation (29-32). RSK phosphorylation by ERK has been shown to activate translation through a variety of substrates including eukaryotic translation initiation factor-4B (eIF4B), tuberous sclerosis complex-1/2 (TSC1/2), the 40S ribosomal subunit protein S6 (rpS6), glycogen synthase kinase-3 (GSK3β), and elongation factor-2 (EF2) kinase (34-40). These studies provide plausible targets linking ERK/RSK to protein translation, but do not provide a potential mechanism for how protein translation enhances anti-nociception. Among the full list of proteins altered by 17-AAG treatment in our proteomic analysis were candidate proteins for this mechanism (data file S1).

These include ion channels like KCNA4 and the CACNA2D1 subunit of the voltage-gated calcium channel, and numerous signaling proteins and signaling protein regulators (such as PLCD3, PP1, RGS12, and GPR162); these provide plausible future candidates to investigate that could link the protein translation we observe to enhanced anti-nociception. One finding which will guide such a search is that any candidate protein must have a rapid turnover half-life, given our observation that inhibiting translation within 30 minutes of opioid treatment abolished the response, suggesting the protein must be degraded sufficiently within that timeframe.

We also observed interesting systemic interactions above the level of molecular circuitry when investigating how Hsp90 inhibition in the brain and spinal cord interact. We found that Hsp90 inhibition in the brain had a dominant effect over that in the spinal cord in terms of the overall behavioral output, with either systemic or combined i.c.v./i.t. inhibition. For example, in the tail flick pain model, brain Hsp90 inhibition had no notable effect on opioid-induced anti-nociception but nonetheless repressed the effects of spinal inhibition. The brain has a well-established circuit of opioidergic descending modulation with cell bodies in the rostroventral medulla and other regions and synapsing on nociceptive modulatory circuits in the spinal cord (49). It may be that descending modulatory neurons in the brain can override the spinal circuits when Hsp90 is inhibited in the brain. Lending some support to this hypothesis is our finding that spinal Hsp90 inhibition leads to enhanced ERK phosphorylation in lamina I/II of the dorsal horn of the spinal cord, which is a key target region for these descending neurons (50). Investigating the circuit context in which Hsp90 regulates anti-nociception will provide key insights into how the molecular circuitry translates into a whole animal behavioral response.

In this study, we demonstrated a spinal cord-specific role for Hsp90 within MOR downstream signaling and, in doing so, have begun to elucidate MOR-dependent downstream

mechanisms of ERK phosphorylation within the spinal cord that can impact systemic morphine-induced anti-nociception. We propose a mechanism in which Hsp90 serves as a brake on ERK phosphorylation within neurons in the spinal cord dorsal horn. Once the brake is removed by a spinal Hsp90 inhibitor, ERK phosphorylation is "unchained" and can contribute to MOR-agonist induced anti-nociception through RSK activation and rapid translation. This translation event must upregulate proteins which contribute to either hyperpolarization or the prevention of neurotransmitter release in primary or secondary nociceptive afferents within the spinal cord, further preventing the transmission of pain signals. This mechanism is not only significant in the context of molecular signaling, but there is also the potential to capitalize on these findings clinically by developing an opioid dose reduction strategy. Hsp90 inhibitors could be used to amplify morphine analgesia through the spinal cord without altering unwanted morphine side effects, many of which are evoked through brain regions such as the striatum (reward) or through the gut (constipation) and would not be affected by spinal cord treatment.

Materials and Methods

Reagents

17-AAG (#AAJ66960MC), DAMGO (#11711), Fmk (#46-901-0), cycloheximide (#AC357420010), and U0126 (#11-445) were all purchased from Fisher Scientific (Waltham, MA). Morphine sulfate pentahydrate was obtained through the National Institute on Drug Abuse Drug Supply Program and distributed through the Research Triangle Institute. KU-32 was synthesized using published protocols, and purity (>95%) and identity confirmed by HPLC and mass spectrometry (25). 17-AAG, U0126, Fmk, KU-32, and cycloheximide were prepared as stock solutions in DMSO, and DAMGO was prepared as a stock solution in water. Morphine was

prepared fresh for each experiment in USP saline. Powders were stored as recommended by the manufacturer, and stock solutions stored at -20°C. Appropriate vehicle controls were used for each experiment: 10% DMSO in water for KU-32, Fmk, and cycloheximide i.t. injections; water for DAMGO i.t. injections; USP saline for systemic morphine injections; and 10% DMSO, 10% Tween-80, and 80% USP saline for the 17-AAG and U0126 i.t., i.c.v., and i.p. injections.

Animals

Male and female CD-1 mice in age-matched controlled cohorts from 4–8 weeks of age were used for all experiments and were obtained from Charles River Laboratories (Wilmington, MA). Male and female mice were used in approximately equal numbers in each experiment; no sex differences were observed, so the male and female cohorts were combined for all data shown. CD-1 (also known as ICR) mice are commonly used in opioid research and in our previous work as a line with a strong response to opioid drugs [as in (21, 51)]. Mice were allowed to recover for at least 5 days after shipment before being used in experiments. The mice were kept in an AAALAC-accredited vivarium at the University of Arizona under temperature control and 12-hour light/dark cycles with food (standard lab chow) and water available *ad libitum*. No more than five mice were kept in a cage. The animals were monitored daily, including after surgical procedures, by trained veterinary staff. All experiments performed were in accordance with IACUC-approved protocols at the University of Arizona and according to the guidelines of the NIH Care and Use of Laboratory Animals handbook.

Behavioral experiments

Prior to any behavioral experiment or testing, the animals were brought to the testing room in their home cages for at least 1 hour for acclimation. Testing always occurred within the same approximate time of day between experiments, and environmental factors (noise, personnel, and scents) were minimized. All testing apparatus (cylinders, grid boxes, etc.) were cleaned between uses. The experimenter was blinded to treatment group by another laboratory member delivering coded drug vials, which were then decoded after collection of all data.

Paw incision and mechanical allodynia

Mechanical thresholds were determined prior to surgery using calibrated Von Frey filaments (Ugo Basile, Varese, Italy) with the up-down method and four measurements after the first response per mouse (21, 52). The mice were housed in a homemade apparatus with Plexiglas walls and ceiling and a wire mesh floor (3”W x 4”L x 3”H with 0.25” wire mesh). The surgery was then performed by anesthesia with ~2% isoflurane in standard air, preparation of the left plantar hind paw with iodine and 70% ethanol, and a 5-mm incision made through the skin and fascia with a no. 11 scalpel. The muscle was elevated with curved forceps leaving the origin and insertion intact, and the muscle was split lengthwise using the scalpel. The wound was then closed with 5-0 polyglycolic acid sutures. All i.c.v. and i.t. injections were performed as described in our previous work (21). For the 17-AAG/KU-32 experiments, the mice were then injected i.t. and left to recover for 24 hours. The next day, the mechanical threshold was again determined as described above, and i.t. injections took place for the U0126 experiments with a 15-min treatment time. Both the 17-AAG and the U0126 mice were then injected with 3.2 mg/kg morphine s.c., and mechanical thresholds were determined over a 3-hour time course. No animals were excluded from these studies.

Tail flick assay

Pre-injection tail-flick baselines were determined in a 52 °C warm water tail-flick assay with a 10 sec cutoff time (21). The mice were then injected i.t. with 17-AAG, KU-32, cycloheximide, Fmk, or U0126 with a 24-hour (17-AAG and KU-32), 30-min (cycloheximide and Fmk), or 15-min (U0126) treatment time. Twenty-four hours after injection, baselines were determined for the 17-AAG experiments. The mice were then injected s.c. with 3.2mg/kg of morphine, and tail-flick latencies were determined over a 2-hour time course. No animals were excluded from these studies.

Rotarod test

Mice were subjected to three training trials of 3 min each on a Rotarod device, with the machine off for trial 1, the machine on but not rotating for trial 2, and the machine rotating at 4 rpm for trial 3 (21). An automatic timer in the unit was used to record fall latencies with a 3-min maximum time. The mice were then injected i.t. with 17-AAG or vehicle and allowed to recover for 24 hours, and another 3-min Rotarod trial was performed without additional treatments or interventions. This trial was done with an accelerating 4–16 rpm task over the 3-min trial time. No mice were excluded from these studies.

Western blotting and analysis

Mouse spinal cord or PAG protein lysates were prepared using our previously published protocol (21) and quantified with a BCA protein quantitation assay using the manufacturer's

protocol (Bio-Rad). The protein was run on precast 10% Bis-Tris Bolt gels (Fisher Scientific #NW00100BOX) using the Bolt gel apparatus and following the manufacturer's instructions. The gels were transferred to nitrocellulose membrane (Bio-Rad) using a wet transfer system (30 V, minimum of 1 hour on ice). The blots were blocked with 5% nonfat dry milk in TBS and incubated with primary antibody in 5% BSA in TBS + 0.1% Tween-20 (TBST) overnight rocking at 4 °C. The blots were then washed three times for 5 min in TBST, incubated with secondary antibody (see below) in 5% milk in TBST for 1 hour of rocking at room temperature, washed again, and imaged with a LiCor Odyssey infrared imaging system (LiCor, Lincoln, NE). Some blots were then stripped with 25 mM glycine-HCl and 1% SDS, pH 2.0, for 30–60 min of rocking at room temperature prior to being washed and re-exposed to primary antibody. The resulting image bands were quantified using Scion Image (based on NIH Image). All images were quantified in the linear signal range, which is easier to ensure because the Odyssey imager is a dynamic imager that allows for fine control of exposure. The pERK signal was normalized to the tERK signal, and pRSK1 and 2 were normalized to tRSK1 and 2 respectively, with both measured from the same blot as the primary target. The normalized intensities were further normalized to a vehicle control present on the same blot.

Immunohistochemistry

Perfusions were performed on drug treated mice with cold PBS, followed with cold 4% paraformaldehyde in PBS. Shortly after the perfusions were complete, fixed spinal cords were extracted and immediately placed in cold 4% paraformaldehyde for ~6 hours. Spinal cords were then placed in 15% sucrose in PBS overnight, followed by 30% sucrose in PBS overnight. Spinal cords were then flash frozen in O.C.T. Compound using liquid nitrogen and sectioned with a

Microm HM 525 cryostat at a thickness of 20 μm between the L5 and L6 vertebrae and mounted on Surgipath X-tra microscope slides. Spinal cord sections were rehydrated in PBS in preparation for free float staining. Samples were incubated in an endogenous peroxidase blocking buffer consisting of 60% methanol and 0.3% H2O2 in PBS at RT for 30 minutes and then washed with PBST. They were then incubated in 5% goat serum, 1% BSA in PBST at RT for 1 hour. Samples were then incubated with 1:5000 primary pERK antibody in 1.5% goat serum, 1% BSA in PBST at 4˚C overnight. Samples were then washed with PBST and then incubated with a 1:400 biotinylated secondary goat anti-rabbit IgG antibody in 1.5% goat serum, 1% BSA in PBST at RT for 1 hour. Samples were prepared as instructed using the Vectastain Elite ABC HRP Kit (#PK-6101) and TSA Plus Fluorescein Evaluation Kit (#NEL741E001KT), both from PerkinElmer. NeuN and MAP2 primary antibodies were used at 1:1000 and 1:500 respectively during the pERK primary incubation. The secondary for NeuN and MAP2 was Alexa Flour goat anti-mouse IgG 594 which was used at 1:500 for both which was added during the pERK secondary incubation mentioned above. Stained spinal cord sections were then mounted onto slides with Novus FluorEver. Sections were imaged at 4x, 10x, and 63x using an Olympus BX51 microscope equipped with a Hamamatsu C8484 digital camera. Images were analyzed using ImageJ. Dorsal horn regions were selected, and average mean intensities were measured and normalized to no primary Ab and vehicle controls within experimental groups.

Antibodies

The antibodies used were: Hsp70 (Cell Signaling 4872S, lot 4, rabbit, 1:1000), GAPDH (ThermoFisher MA5-15738, lot PI209504, mouse, 1:1000), pERK (Cell Signaling 4370S, lot 12, rabbit, 1:1000 for Westerns and 1:5000 for IHC), tERK (Cell Signaling 4696S, lot 16, mouse,

1:1000), pRSK1 (Cell Signaling 11989S, lot 4, rabbit 1:1000), tRSK1 (Cell Signaling 8408S, lot 5, rabbit 1:1000), pRSK2 (Cell Signaling 3556S, lot 4, rabbit, 1:1000), tRSK2 (Cell Signaling 5528S, lot 1, rabbit 1:1000), MAP2 (Invitrogen 13-1500, lot TJ275359, mouse, 1:500), NeuN (Abcam ab104224, lot GR3247200-1, mouse, 1:1000), secondary GαM680 (LiCor 926-68020, lot C50721-02, goat, 1:10,000–1:20,000), secondary GαR800 (LiCor 926-32211, lot C50602–05, goat, 1:10,000–1:20,000), and secondary Alexa Fluor goat anti-mouse IgG 594 (Invitrogen A11032, lot 1985396, mouse, 1:500).

Proteomics - In-gel digestion

Mouse spinal cord protein lysates (100 μg) were prepared as for Western blot from animals that were treated with either 17-AAG or vehicle (N = 3 each) and were separated on a 10% SDS-PAGE gel and stained with Bio-Safe Coomassie G-250 Stain. Each lane of the SDS-PAGE gel was cut into six slices and the gel slices were subjected to trypsin digestion. The resulting peptides were purified by C18-based desalting exactly as previously described (53, 54).

Proteomics - Mass spectrometry and database search

HPLC-ESI-MS/MS was performed in positive ion mode on a Thermo Scientific Orbitrap Fusion Lumos tribrid mass spectrometer fitted with an EASY-Spray Source (Thermo Scientific, San Jose, CA). NanoLC was performed exactly as previously described (53, 54). Tandem mass spectra were extracted from Xcalibur 'RAW' files and charge states were assigned using the ProteoWizard 3.0 msConvert script using the default parameters. The fragment mass spectra were searched against the *Mus musculus* SwissProt_2018_01 database (16965 entries) using Mascot

(Matrix Science, London, UK; version 2.6.0) using the default probability cut-off score. The search variables that were used were: 10 ppm mass tolerance for precursor ion masses and 0.5 Da for product ion masses; digestion with trypsin; a maximum of two missed tryptic cleavages; variable modifications of oxidation of methionine and phosphorylation of serine, threonine, and tyrosine. Cross-correlation of Mascot search results with X! Tandem was accomplished with Scaffold (version Scaffold_4.8.7; Proteome Software, Portland, OR, USA). Probability assessment of peptide assignments and protein identifications were made using Scaffold. Only peptides with ≥ 95% probability were considered. The mass spectrometry proteomics data have been deposited to the ProteomeXchange Consortium via the PRIDE (55, 56) partner repository with the dataset identifier PXD015060 and 10.6019/PXD015060. The reviewer account details are Username: reviewer97855@ebi.ac.uk and Password: 8AM00kfd.

Label-free quantitative proteomics

Progenesis QI for proteomics software (version 2.4, Nonlinear Dynamics Ltd., Newcastle upon Tyne, UK) was used to perform ion-intensity based label-free quantification as previously described (54). In an automated format, .RAW files were imported and converted into two-dimensional maps (y-axis = time, x-axis = m/z) followed by selection of a reference run for alignment purposes. An aggregate data set containing all peak information from all samples was created from the aligned runs, which was then further narrowed down by selecting only +2, +3, and +4 charged ions for further analysis. The samples were then grouped and a peak list of fragment ion spectra from only the top eight most intense precursors of a feature was exported to a Mascot generic file (.MGF) format and searched using Mascot (Matrix Science, London, UK; version 2.4) with the same search variables as described above. The resulting Mascot .XML file

was then imported into Progenesis, allowing for peptide/protein assignment, while peptides with a Mascot Ion Score of <25 were not considered for further analysis. Protein quantification was performed using only non-conflicting peptides and precursor ion-abundance values were normalized in a run to those in a reference run (not necessarily the same as the alignment reference run).

Statistical analysis

All data were reported as the mean ± SEM and normalized where appropriate as described above to total protein and/or Vehicle control groups. The behavioral data were reported raw without maximum possible effect (MPE) or other normalization. Biological and technical replicates are described in the Figure Legends. Comparisons between two groups (HSP70 protein expression) were performed by unpaired 2-tailed *t* tests. Comparisons of more than two groups (ERK and RSK signaling, paw incision, tail flick, and rotarod) were performed by two-way ANOVA with Sidak's (behavior) or Tukey's (Western) post hoc tests. In all cases, significance was defined as $p < 0.05$. All graphing and statistical analyses were performed using GraphPad Prism 8.1 (San Diego, CA).

Supplementary Materials

Data file S1. Full set of proteomic analysis results.

Data file S2. Individual proteomic analysis results for GO/KEGG analysis.

References and Notes:

1. Gaskin, D. J., and P. Richard. 2012. The economic costs of pain in the United States. *J Pain* 13: 715-724.
2. Johannes, C. B., T. K. Le, X. Zhou, J. A. Johnston, and R. H. Dworkin. 2010. The prevalence of chronic pain in United States adults: results of an Internet-based survey. *The journal of pain : official journal of the American Pain Society* 11: 1230-1239.
3. National Collaborating Centre for, C. 2012. National Institute for Health and Clinical Excellence: Guidance. In *Opioids in Palliative Care: Safe and Effective Prescribing of Strong Opioids for Pain in Palliative Care of Adults*. National Collaborating Centre for Cancer (UK)

Copyright 2012, (c) National Collaborating Centre for Cancer., Cardiff (UK).

4. Fields, H. L. 2011. The doctor's dilemma: opiate analgesics and chronic pain. *Neuron* 69: 591-594.
5. Goodyear, K., C. L. Haass-Koffler, and D. Chavanne. 2018. Opioid use and stigma: The role of gender, language and precipitating events. *Drug Alcohol Depend* 185: 339-346.
6. Al-Hasani, R., and M. R. Bruchas. 2011. Molecular mechanisms of opioid receptor-dependent signaling and behavior. *Anesthesiology* 115: 1363-1381.
7. Madariaga-Mazon, A., A. F. Marmolejo-Valencia, Y. Li, L. Toll, R. A. Houghten, and K. Martinez-Mayorga. 2017. Mu-Opioid receptor biased ligands: A safer and painless discovery of analgesics? *Drug discovery today* 22: 1719-1729.

8. Olson, K. M., W. Lei, A. Keresztes, J. LaVigne, and J. M. Streicher. 2017. Novel Molecular Strategies and Targets for Opioid Drug Discovery for the Treatment of Chronic Pain. *Yale J Biol Med* 90: 97-110.

9. Villanueva, M. T. 2017. Analgesia: Designing out opioid side effects. *Nature reviews. Drug discovery* 16: 311.

10. Liang, D. Y., W. W. Li, C. Nwaneshiudu, K. A. Irvine, and J. D. Clark. 2018. Pharmacological Characters of Oliceridine, a mu-Opioid Receptor G-Protein[FIGURE DASH]Biased Ligand in Mice. *Anesthesia and analgesia*.

11. Drieu la Rochelle, A., K. Guillemyn, M. Dumitrascuta, C. Martin, V. Utard, R. Quillet, S. Schneider, F. Daubeuf, T. Willemse, P. Mampuys, B. U. W. Maes, N. Frossard, F. Bihel, M. Spetea, F. Simonin, and S. Ballet. 2018. A bifunctional-biased mu-opioid agonist-neuropeptide FF receptor antagonist as analgesic with improved acute and chronic side effects. *Pain*.

12. Manglik, A., H. Lin, D. K. Aryal, J. D. McCorvy, D. Dengler, G. Corder, A. Levit, R. C. Kling, V. Bernat, H. Hubner, X. P. Huang, M. F. Sassano, P. M. Giguere, S. Lober, D. Da, G. Scherrer, B. K. Kobilka, P. Gmeiner, B. L. Roth, and B. K. Shoichet. 2016. Structure-based discovery of opioid analgesics with reduced side effects. *Nature* 537: 185-190.

13. Wang, Y., Y. H. Ge, Y. X. Wang, T. Liu, P. Y. Law, H. H. Loh, H. Z. Chen, and Y. Qiu. 2015. Modulation of mTOR Activity by mu-Opioid Receptor is Dependent upon the Association of Receptor and FK506-Binding Protein 12. *CNS neuroscience & therapeutics* 21: 591-598.

14. Bao, Y., Y. Gao, W. Hou, L. Yang, X. Kong, H. Zheng, C. Li, and B. Hua. 2015. Engagement of signaling pathways of protease-activated receptor 2 and mu-opioid receptor

in bone cancer pain and morphine tolerance. *International journal of cancer* 137: 1475-1483.

15. Li, J., and J. Buchner. 2013. Structure, function and regulation of the hsp90 machinery. *Biomedical journal* 36: 106-117.

16. Eckl, J. M., and K. Richter. 2013. Functions of the Hsp90 chaperone system: lifting client proteins to new heights. *International journal of biochemistry and molecular biology* 4: 157-165.

17. Kaigorodova, E. V., and M. V. Bogatyuk. 2014. Heat shock proteins as prognostic markers of cancer. *Current cancer drug targets* 14: 713-726.

18. Schulz, R., and U. M. Moll. 2014. Targeting the heat shock protein 90: a rational way to inhibit macrophage migration inhibitory factor function in cancer. *Current opinion in oncology* 26: 108-113.

19. Jhaveri, K., S. O. Ochiana, M. P. Dunphy, J. F. Gerecitano, A. D. Corben, R. I. Peter, Y. Y. Janjigian, E. M. Gomes-DaGama, J. Koren, 3rd, S. Modi, and G. Chiosis. 2014. Heat shock protein 90 inhibitors in the treatment of cancer: current status and future directions. *Expert opinion on investigational drugs* 23: 611-628.

20. Streicher, J. M. 2019. The Role of Heat Shock Proteins in Regulating Receptor Signal Transduction. *Mol Pharmacol* 95: 468-474.

21. Lei, W., N. Mullen, S. McCarthy, C. Brann, P. Richard, J. Cormier, K. Edwards, E. J. Bilsky, and J. M. Streicher. 2017. Heat-shock protein 90 (Hsp90) promotes opioid-induced anti-nociception by an ERK mitogen-activated protein kinase (MAPK) mechanism in mouse brain. *J Biol Chem* 292: 10414-10428.

22. Chiosis, G., C. A. Dickey, and J. L. Johnson. 2013. A global view of Hsp90 functions. *Nature structural & molecular biology* 20: 1-4.

23. McClellan, A. J., Y. Xia, A. M. Deutschbauer, R. W. Davis, M. Gerstein, and J. Frydman. 2007. Diverse cellular functions of the Hsp90 molecular chaperone uncovered using systems approaches. *Cell* 131: 121-135.

24. Thanomkitti, K., K. Fong-Ngern, K. Sueksakit, R. Thuangtong, and V. Thongboonkerd. 2018. Molecular functional analyses revealed essential roles of HSP90 and lamin A/C in growth, migration, and self-aggregation of dermal papilla cells. *Cell Death Discov* 4: 53.

25. Burlison, J. A., L. Neckers, A. B. Smith, A. Maxwell, and B. S. Blagg. 2006. Novobiocin: redesigning a DNA gyrase inhibitor for selective inhibition of hsp90. *J Am Chem Soc* 128: 15529-15536.

26. Ansar, S., J. A. Burlison, M. K. Hadden, X. M. Yu, K. E. Desino, J. Bean, L. Neckers, K. L. Audus, M. L. Michaelis, and B. S. Blagg. 2007. A non-toxic Hsp90 inhibitor protects neurons from Abeta-induced toxicity. *Bioorg Med Chem Lett* 17: 1984-1990.

27. Smith, V., E. A. Sausville, R. F. Camalier, H. H. Fiebig, and A. M. Burger. 2005. Comparison of 17-dimethylaminoethylamino-17-demethoxy-geldanamycin (17DMAG) and 17-allylamino-17-demethoxygeldanamycin (17AAG) in vitro: effects on Hsp90 and client proteins in melanoma models. *Cancer chemotherapy and pharmacology* 56: 126-137.

28. Kwon, H. M., Y. Kim, S. I. Yang, Y. J. Kim, S. H. Lee, and B. W. Yoon. 2008. Geldanamycin protects rat brain through overexpression of HSP70 and reducing brain edema after cerebral focal ischemia. *Neurological research* 30: 740-745.

29. Cargnello, M., and P. P. Roux. 2011. Activation and function of the MAPKs and their substrates, the MAPK-activated protein kinases. *Microbiology and molecular biology reviews : MMBR* 75: 50-83.

30. Gehart, H., S. Kumpf, A. Ittner, and R. Ricci. 2010. MAPK signalling in cellular metabolism: stress or wellness? *EMBO reports* 11: 834-840.

31. Pal, J. K. 1998. Hsp90 regulates protein synthesis by activating the heme-regulated eukaryotic initiation factor 2α (eIF-2α) kinase in rabbit reticulocyte lysates. *Journal of Biosciences* 23: 353-360.

32. Uma, S., S. D. Hartson, J. J. Chen, and R. L. Matts. 1997. Hsp90 is obligatory for the heme-regulated eIF-2alpha kinase to acquire and maintain an activable conformation. *J Biol Chem* 272: 11648-11656.

33. Darcq, E., K. Befort, P. Koebel, S. Pannetier, M. K. Mahoney, C. Gaveriaux-Ruff, A. Hanauer, and B. L. Kieffer. 2012. RSK2 signaling in medial habenula contributes to acute morphine analgesia. *Neuropsychopharmacology* 37: 1288-1296.

34. Roux, P. P., B. A. Ballif, R. Anjum, S. P. Gygi, and J. Blenis. 2004. Tumor-promoting phorbol esters and activated Ras inactivate the tuberous sclerosis tumor suppressor complex via p90 ribosomal S6 kinase. *Proc Natl Acad Sci U S A* 101: 13489-13494.

35. Shahbazian, D., P. P. Roux, V. Mieulet, M. S. Cohen, B. Raught, J. Taunton, J. W. Hershey, J. Blenis, M. Pende, and N. Sonenberg. 2006. The mTOR/PI3K and MAPK pathways converge on eIF4B to control its phosphorylation and activity. *The EMBO journal* 25: 2781-2791.

36. Roux, P. P., D. Shahbazian, H. Vu, M. K. Holz, M. S. Cohen, J. Taunton, N. Sonenberg, and J. Blenis. 2007. RAS/ERK signaling promotes site-specific ribosomal protein S6

phosphorylation via RSK and stimulates cap-dependent translation. *J Biol Chem* 282: 14056-14064.

37. Sutherland, C., I. A. Leighton, and P. Cohen. 1993. Inactivation of glycogen synthase kinase-3 beta by phosphorylation: new kinase connections in insulin and growth-factor signalling. *The Biochemical journal* 296 (Pt 1): 15-19.

38. Cohen, P., and S. Frame. 2001. The renaissance of GSK3. *Nature Reviews Molecular Cell Biology* 2: 769-776.

39. Wang, X., W. Li, M. Williams, N. Terada, D. R. Alessi, and C. G. Proud. 2001. Regulation of elongation factor 2 kinase by p90(RSK1) and p70 S6 kinase. *The EMBO journal* 20: 4370-4379.

40. Anjum, R., and J. Blenis. 2008. The RSK family of kinases: emerging roles in cellular signalling. *Nature reviews. Molecular cell biology* 9: 747-758.

41. Macey, T. A., J. D. Lowe, and C. Chavkin. 2006. Mu opioid receptor activation of ERK1/2 is GRK3 and arrestin dependent in striatal neurons. *The Journal of biological chemistry* 281: 34515-34524.

42. Duraffourd, C., E. Kumala, L. Anselmi, N. C. Brecha, and C. Sternini. 2014. Opioid-induced mitogen-activated protein kinase signaling in rat enteric neurons following chronic morphine treatment. *PLoS One* 9: e110230.

43. Gutstein, H. B., E. A. Rubie, A. Mansour, H. Akil, and J. R. Woodgett. 1997. Opioid effects on mitogen-activated protein kinase signaling cascades. *Anesthesiology* 87: 1118-1126.

44. Schmidt, H., S. Schulz, M. Klutzny, T. Koch, M. Handel, and V. Hollt. 2000. Involvement of mitogen-activated protein kinase in agonist-induced phosphorylation of the mu-opioid receptor in HEK 293 cells. *J Neurochem* 74: 414-422.

45. Chen, Y., C. Geis, and C. Sommer. 2008. Activation of TRPV1 contributes to morphine tolerance: involvement of the mitogen-activated protein kinase signaling pathway. *J Neurosci* 28: 5836-5845.

46. Popiolek-Barczyk, K., W. Makuch, E. Rojewska, D. Pilat, and J. Mika. 2014. Inhibition of intracellular signaling pathways NF-kappaB and MEK1/2 attenuates neuropathic pain development and enhances morphine analgesia. *Pharmacol Rep* 66: 845-851.

47. Kim, N., J. Y. Kim, and M. A. Yenari. 2015. Pharmacological induction of the 70-kDa heat shock protein protects against brain injury. *Neuroscience* 284: 912-919.

48. Wang, Y., and S. R. McAlpine. 2015. Heat-shock protein 90 inhibitors: will they ever succeed as chemotherapeutics? *Future Med Chem* 7: 87-90.

49. Ossipov, M. H., J. Lai, T. P. Malan, Jr., and F. Porreca. 2000. Spinal and supraspinal mechanisms of neuropathic pain. *Ann N Y Acad Sci* 909: 12-24.

50. Heinricher, M. M., I. Tavares, J. L. Leith, and B. M. Lumb. 2009. Descending control of nociception: Specificity, recruitment and plasticity. *Brain Res Rev* 60: 214-225.

51. Ananthan, S., S. K. Saini, C. M. Dersch, H. Xu, N. McGlinchey, D. Giuvelis, E. J. Bilsky, and R. B. Rothman. 2012. 14-Alkoxy- and 14-acyloxypyridomorphinans: mu agonist/delta antagonist opioid analgesics with diminished tolerance and dependence side effects. *J Med Chem* 55: 8350-8363.

52. Chaplan, S. R., F. W. Bach, J. W. Pogrel, J. M. Chung, and T. L. Yaksh. 1994. Quantitative assessment of tactile allodynia in the rat paw. *J Neurosci Methods* 53: 55-63.

53. Kruse, R., J. Krantz, N. Barker, R. L. Coletta, R. Rafikov, M. Luo, K. Hojlund, L. J. Mandarino, and P. R. Langlais. 2017. Characterization of the CLASP2 Protein Interaction

Network Identifies SOGA1 as a Microtubule-Associated Protein. *Molecular & cellular proteomics : MCP* 16: 1718-1735.

54. Parker, S. S., J. Krantz, E. A. Kwak, N. K. Barker, C. G. Deer, N. Y. Lee, G. Mouneimne, and P. R. Langlais. 2019. Insulin Induces Microtubule Stabilization and Regulates the Microtubule Plus-end Tracking Protein Network in Adipocytes. *Molecular & cellular proteomics : MCP* 18: 1363-1381.

55. Deutsch, E. W., A. Csordas, Z. Sun, A. Jarnuczak, Y. Perez-Riverol, T. Ternent, D. S. Campbell, M. Bernal-Llinares, S. Okuda, S. Kawano, R. L. Moritz, J. J. Carver, M. Wang, Y. Ishihama, N. Bandeira, H. Hermjakob, and J. A. Vizcaino. 2017. The ProteomeXchange consortium in 2017: supporting the cultural change in proteomics public data deposition. *Nucleic Acids Res* 45: D1100-D1106.

56. Perez-Riverol, Y., A. Csordas, J. Bai, M. Bernal-Llinares, S. Hewapathirana, D. J. Kundu, A. Inuganti, J. Griss, G. Mayer, M. Eisenacher, E. Perez, J. Uszkoreit, J. Pfeuffer, T. Sachsenberg, S. Yilmaz, S. Tiwary, J. Cox, E. Audain, M. Walzer, A. F. Jarnuczak, T. Ternent, A. Brazma, and J. A. Vizcaino. 2019. The PRIDE database and related tools and resources in 2019: improving support for quantification data. *Nucleic Acids Res* 47: D442-D450.

Acknowledgments: We would like to acknowledge Dr. Tally Largent-Milnes for assistance in analysing the spinal cord IHC results, and Dr. Todd Vanderah for sharing his Rotarod device. **Funding**: This work was funded by an Arizona Biomedical Research Commission New Investigator Award #ADHS18-198875 and institutional funds from the University of Arizona, both to JMS. **Author contributions**: DID performed and analyzed most of the experiments, participated in project and experimental design, and co-wrote the manuscript. WL performed and analyzed the systemic behavioral experiments. NKB performed and analyzed the quantitative proteomic experiments. CS performed and analyzed some of the co-staining IHC experiments. SM synthesized and purified KU-32. BSJB supervised SM in the performance of the chemical synthesis and participated in project design. PRL supervised NKB in the performance of the proteomic experiments and participated in experimental and project design. JMS supervised DID, WL, and CS in the performance of their work, secured funding for the project, conceived the initial idea of the project, participated in experimental and project design, and co-wrote the manuscript. All authors had editorial input into the manuscript. **Competing interests**: The authors declare they have no competing interests. **Data and materials availability**: A material transfer agreement is required for the molecules used in this study and quantity is limited (BSJB). The full results of the proteomic analysis are contained in the supplementary materials and have been uploaded to the ProteomeXchange Consortium via the PRIDE (55, 56) partner repository: PXD015060 and 10.6019/PXD015060. All other data needed to evaluate the conclusions in the paper are present in the paper or the Supplementary Materials.

Figure Legends

Fig. 1 – Spinal cord Hsp90 inhibition enhances morphine anti-nociception. (A to E) Male and female CD-1 mice were treated as indicated in the labels with either 17-AAG (0.5 nmol) or KU-32 (0.01 nmol; C), or vehicle injected by the intracerebroventricular (icv) or intrathecal (it) route, followed by a 24-hour recovery and then injected subcutaneously with or without morphine (Mor; A to D, 3.2 mg/kg; E, 3.2 or 10 mg/kg) and subjected to behavioral testing. BL = baseline response. Data are mean ± SEM from N = number of mice per group noted on each graph; each experiment was performed with one (D), two (A to C) or three (E) independent technical replicates (meaning groups of mice performed on different days). * $p < 0.05$, *** $p < 0.001$, **** $p < 0.0001$ vs. same time point in Vehicle group, by two-way ANOVA with Sidak's post hoc test.

Fig. 2 – Brain Hsp90 inhibition overrides spinal cord Hsp90 inhibition with respect to opioid anti-nociception. (A and B) Representative images (A) and analysis (B) of Western blotting for Hsp70 in the periaqueductal grey (PAG) and spinal cord (SC) from male and female CD-1 mice that had received intraperitoneal (ip) injection with 50 mg/kg 17-AAG or vehicle with a 24 hour recovery. Hsp70 densitometry was normalized to that of GAPDH (loading control) from each sample and was further normalized to the vehicle group within each tissue. Data are mean ± SEM of N = 9-10 mice, performed with two technical replicates. ** $p < 0.01$ vs. same tissue in vehicle group, by unpaired two-tailed *t* test. **(C and D)** Tail flick (C) and paw incision (D) pain behavior tests in mice injected with 50 mg/kg 17-AAG or vehicle intraperitoneally (ip), followed by a 24-hour recovery and then a subcutaneous injection of 3.2 mg/kg morphine. Data are mean ± SEM of N = number of mice per group, noted on each graph, performed with 4 (C) or 2 (D) technical

replicates. * $p < 0.05$, **** $p < 0.0001$ vs. same time point in the 17-AAG group, by two-way ANOVA with Sidak's post-hoc test. **(E and F)** Tail flick (E) and paw incision (F) pain behavior tests in mice that received both intracerebroventricular (icv) and intrathecal (it) injections of 0.5 nmol 17-AAG or vehicle, followed by a 24-hour recovery and then a subcutaneous injection of 3.2 mg/kg morphine. Data are mean ± SEM of N = number of mice per group, noted on each graph, performed with 2 technical replicates. * $p < 0.05$, **** $p < 0.0001$ vs. same time point in the 17-AAG group, by two-way ANOVA with Sidak's post-hoc test.

Fig. 3 – Spinal Hsp90 inhibition enables opioid activation of ERK MAPK signaling, leading to enhanced anti-nociception. (A to C) Representative images (A) and analysis (B and C) of Western blotting for phosphorylated ERK (pERK) and Hsp70 in the spinal cord from male and female CD-1 mice injected intrathecally (i.t.) with 0.5 nmol 17-AAG or vehicle followed by a 24-hour recovery and then 0.1 nmol DAMGO or vehicle (Veh) i.t. for 10 min. Densitometry of pERK was normalized to that of total ERK (tERK) within each sample, and the densitometry of Hsp70 was normalized to that of GAPDH; each was further normalized to that in the Vehicle/Vehicle group. Data are mean ± SEM from N = the number of mice per group noted on the graphs, each performed as 4 technical replicates. In (B), * $p < 0.05$ and **** $p < 0.0001$ vs. Vehicle/Vehicle group, and ## $p < 0.01$ vs. 17-AAG/Vehicle group; both by two-way ANOVA with Tukey's post hoc test. In (C), $p > 0.05$ by unpaired two-tailed *t* test. **(D)** Immunohistochemistry (IHC) for pERK (green) performed on L4-L6 region spinal cord tissue from mice treated as described in (A). Representative images from N = 9-10mice/group are shown. **(E and F)** Assessment of colocalization (yellow staining; white arrow) of pERK (green) with neuronal markers NeuN or MAP2 (red) by IHC of the dorsal horn region from 17-AAG/DAMGO-treated mice.

Representative images from N ≥ 3 individual spinal cords per target, each performed as two independent technical replicates. Higher magnification images (63x) are shown in (F). **(G)** Quantitation of the pERK signal in the dorsal horn region from all four groups in (D). Intensity values were normalized to the Vehicle/Vehicle group. N = 9-10 mice per group, each performed in 4 independent technical replicates. ** $p < 0.01$ vs. Vehicle/Vehicle group by two-way ANOVA with Tukey's post hoc test. **(H and I)** Tail flick (H) and paw incision (I) pain behavior tests in mice treated with 0.5 nmol 17-AAG or vehicle (Veh) i.t. for 24 hours, followed by 5 μg U0126 or vehicle i.t. for 15 min, followed by 3.2 mg/kg morphine s.c.. Data are mean ± SEM from N = the number of mice per group noted on the graphs, each performed as 4 (H) or 3 (I) independent technical replicates.* $p < 0.05$, ** $p < 0.01$, *** $p < 0.001$, **** = $p < 0.0001$ vs. same time point in the Veh/Veh group by two-way ANOVA with Sidak's post hoc test..

Fig. 4 – Spinal Hsp90 inhibition evokes rapid protein translation that mediates enhanced morphine-evoked anti-nociception. (A) Tail flick assay on male and female CD-1 mice injected with 0.5 nmol 17-AAG or vehicle (Veh) i.t. for 24 hours, then 85 nmol cycloheximide (CX) or vehicle i.t. for 30 min, then 3.2 mg/kg morphine s.c.. * $p < 0.05$, ** $p < 0.01$, *** $p < 0.001$ vs. corresponding Veh/Veh data; # $p < 0.05$, ## $p < 0.01$ vs. corresponding 17-AAG/CX data; by two-way ANOVA with Sidak's post hoc test. Data are mean ± SEM from N= the number of mice per group as noted in the graph, each performed as four technical replicates. **(B and C)** Western blotting and densitometry analysis of phosphorylated ERK (pERK) abundance in the spinal cords of mice treated i.t. with 17-AAG then CX or vehicle as in (A), followed by 0.1 nmol DAMGO or vehicle for 10 min. pERK density was normalized to total ERK (tERK) density in each sample, and further normalized to the 17-AAG/Vehicle/Vehicle group. * $p < 0.05$ vs. 17-

AAG/Vehicle/Vehicle; # $p < 0.05$ vs. 17-AAG/CX/Vehicle; both by two-way ANOVA with Tukey's post hoc test. Data are mean ± SEM from N= the number of mice per group as noted in the graph, each performed as six technical replicates.

Fig. 5 – Quantitative proteomic analysis reveals a protein network altered by spinal Hsp90 inhibition. (A) Protein sample preparation and proteomic analysis workflow, as detailed in the Methods. The samples were prepared using female CD-1 mice (N=3 per group), which were injected with 0.5 nmol 17-AAG or vehicle i.t. for 24 hours. Spinal cords were removed for proteomic analysis and protein extracted as for Western blotting, detailed in the Methods. These samples were used for all subsequent analysis in this Figure. **(B)** Unbiased hierarchical clustering and heat map analysis of proteins significantly altered by 17-AAG treatment ($p < 0.05$). Red = increased; green = decreased; rows = individual proteins; columns = individual samples. Protein quantity traces for all proteins in each sample are shown, right insets. **(C)** Protein quantity data for the protein kinase RSK2, shown as mean ± SEM of N = 3 per group. * $p < 0.05$ by unpaired two-tailed *t* test. **(D)** Principal component analysis of the full proteomic data set was performed. Both treatment groups cluster together and are well-separated along Component 1, accounting for 75.1% of the variance. Within-group variance only occurs along Component 2, accounting for only 8.5% of the variance. **(E)** Volcano plot of all detected proteins from the full proteomic data set, plotting p-value vs. fold change. Red = significantly downregulated; blue = significantly upregulated; grey = not significant. **(F)** Gene ontology (GO) and KEGG pathway analysis of significantly altered proteins from (B) (see Methods for details). Data are plotted as significance vs. fold enrichment.

Fig. 6 – Spinal Hsp90 inhibition activates RSK1/2 phosphorylation, which mediates enhanced morphine-evoked anti-nociception. (A) Tail flick assay in male and female CD-1 mice injected with 0.5 nmol 17-AAG or vehicle i.t. for 24 hours, followed by 10 nmol Fmk or vehicle i.t. for 30 min, followed by 3.2 mg/kg morphine s.c.. Data are mean ± SEM from N = number of mice per group noted in the graph, each as three technical replicates. ** $p < 0.01$, *** $p < 0.001$, **** $p < 0.0001$ vs. same time point Vehicle/Vehicle group by two-way ANOVA with Sidak's post hoc test. **(B to D)** Western blotting for phosphorylated (p) and total (t) RSK1 and RSK2 in the spinal cords from mice injected with 0.5 nmol 17-AAG or Vehicle i.t. for 24 hours, followed by 0.1 nmol DAMGO or Vehicle i.t. for 10 min. Densitometry of pRSK1 (C) and pRSK2 (D) was normalized to the corresponding tRSK within each sample, and further normalized to the Vehicle/Vehicle group. Data are mean ± SEM from N = number of mice per group noted in the graph, each as three technical replicates. * $p < 0.05$, *** $p < 0.001$, **** $p < 0.0001$ vs. Vehicle/Vehicle group; ## $p < 0.01$ vs. 17-AAG/Vehicle group; both by two-way ANOVA with Tukey's post hoc test.

Fig. 7 – Proposed model of Hsp90 regulation of opioid signaling in the spinal cord. Our data suggest that phosphorylation of ERK-MAPK proteins in the spinal cord by the MOR in response to opioids is blocked by Hsp90. Thus, Hsp90 inhibition (by 17-AAG or KU-32) enables ERK MAPK phosphorylation by the MOR with opioid treatment, leading to an ERK-RSK-translation cascade that promotes opioid anti-nociception.

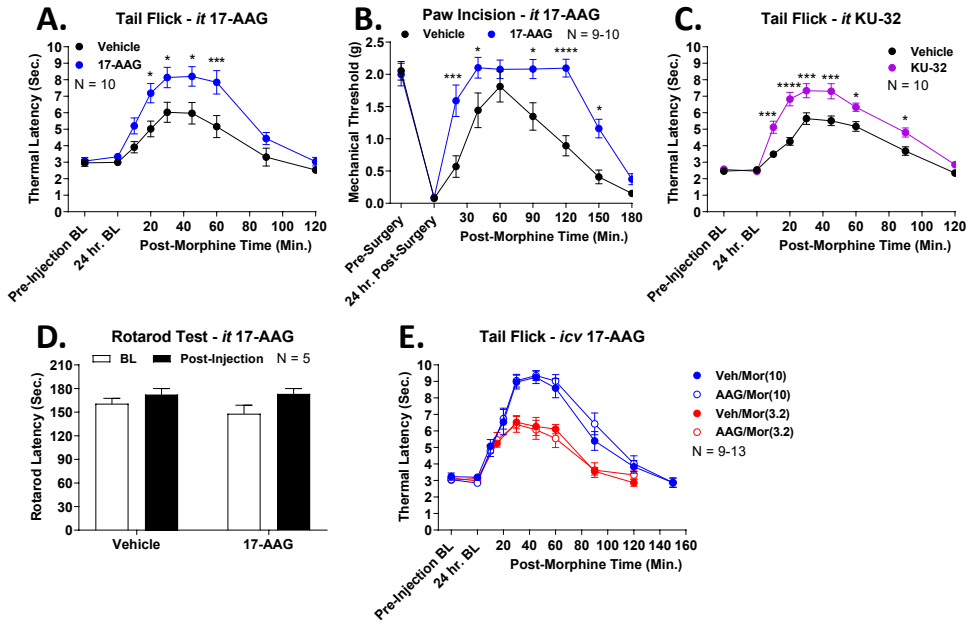

Figure 1 – Basic Behavioral Findings + Controls

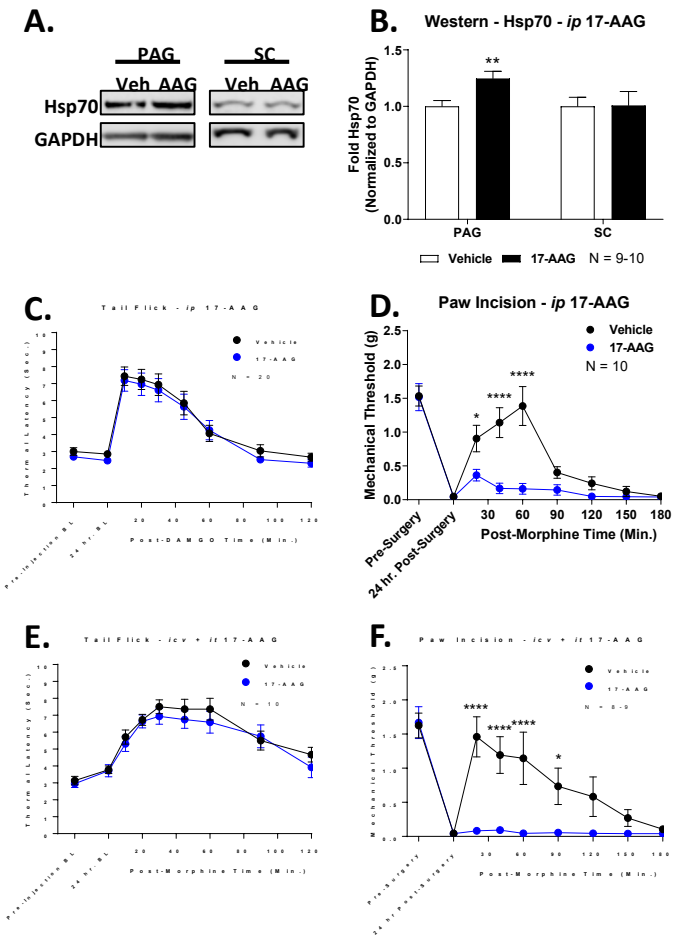

Figure 2 – Systemic Admin/ co admin

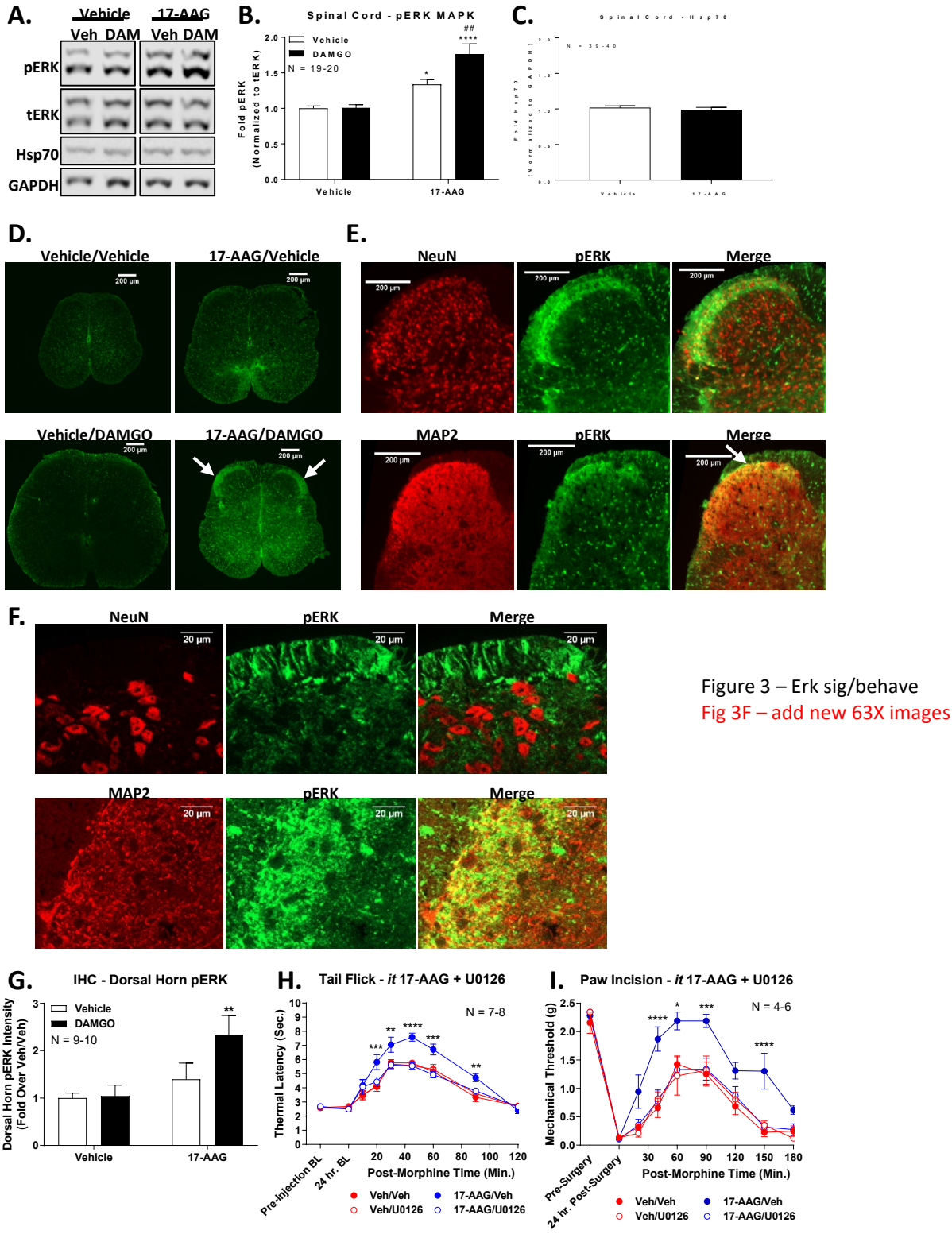

Figure 3 – Erk sig/behave

Fig 3F – add new 63X images

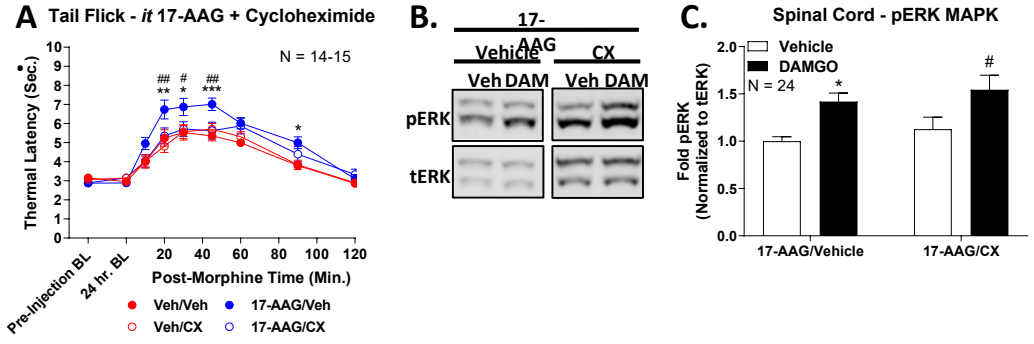

Figure 4 – Protein translation

Figure 5 – Proteomics

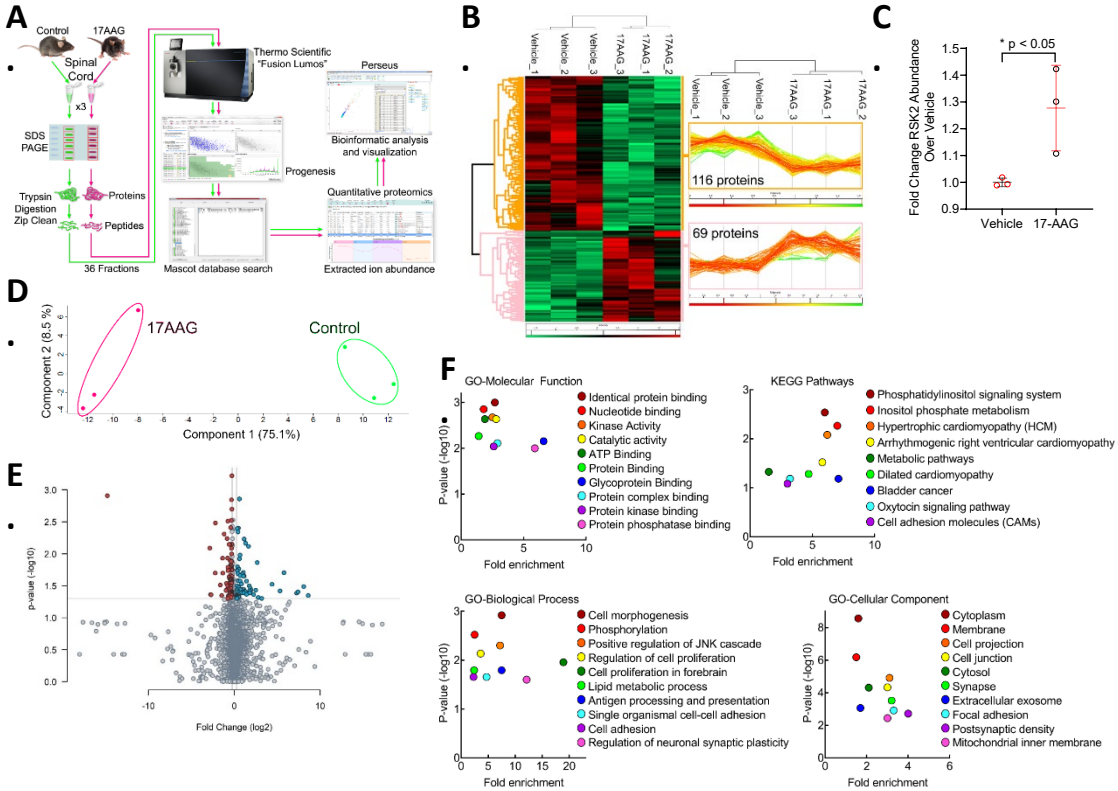

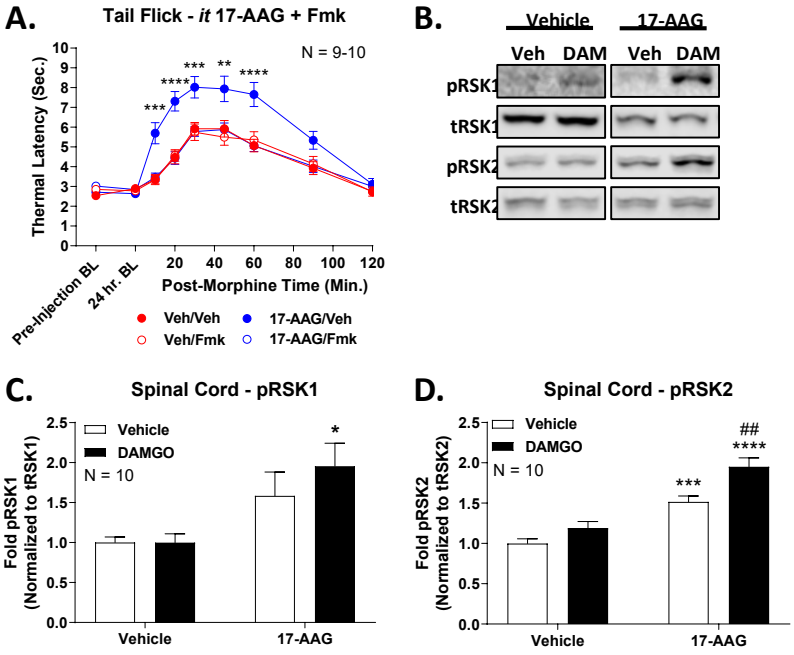

Figure 6 – RSK phosphorylation

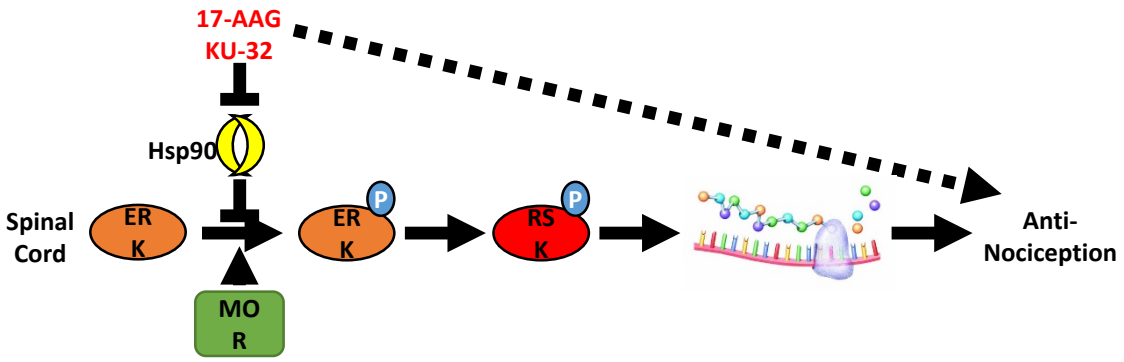

Figure 7 – Model